Inorganic Chemistry
Article

Inorg. Chem. **2010**, *49*, 2765–2772 **2765**
DOI: 10.1021/ic901985z

Series of $M^{I}[Co(bpy)_3][Mo(CN)_8]\cdot nH_2O$ (M^{I} = Li (1), K (2), Rb (3), Cs (4); n = 7−8) Exhibiting Reversible Diamagnetic to Paramagnetic Transition Coupled with Dehydration−Rehydration Process

Marcin Kozieł,[†] Robert Podgajny,[†] Rafał Kania,[‡] Rémy Lebris,[§] Corine Mathonière,*[,§] Krzysztof Lewiński,[†] Krzysztof Kruczała,[†] Michał Rams,[⊥] Christine Labrugère,[§,∥] Azzedine Bousseksou,[⊗] and Barbara Sieklucka*[,†]

[†]*Faculty of Chemistry, Jagiellonian University, Ingardena 3, 30-060 Kraków, Poland,* [‡]*Department of Physics, SUPA, University of Strathclyde, Glasgow G4 0NG, Scotland, U.K.,* [§]*Institut de Chimie de la Matière Condensée de Bordeaux, UPR CNRS No. 9048 − Université Bordeaux, Groupe des Sciences Moléculaires,87 Av. Doc. A. Schweitzer, F-33608 Pessac, France,* [∥]*CeCaMA (Centre de Caractérisation des Matériaux Avancés), Institut de Chimie de la Matière Condensée de Bordeaux, UPR CNRS No. 9048, 87 Av. Doc. A. Schweitzer, F-33608 Pessac, France,* [⊥]*M. Smoluchowski Institute of Physics, Jagiellonian University, Reymonta 4, 31-059 Kraków, Poland, and* [⊗]*Laboratoire de Chimie de Coordination, UPR CNRS No. 8241, 205 route de Narbonne, 31077 Toulouse cedex 04, France*

Received October 7, 2009

In this paper we report the synthesis and the structural and magnetic properties of the series of ionic compounds with general formula: $M^{I}[Co(bpy)_3][Mo(CN)_8]\cdot nH_2O$ (M^{I} = Li, n = 8 (**1**), M^{I} = K, n = 8 (**2**), M^{I} = Rb, n = 8 (**3**), M^{I} = Cs, n = 7.5 (**4**)). Solids **1**−**4** are characterized by the optical outer-sphere metal-to-metal charge transfer (MMCT) transition from Mo(IV) center to Co(III) center in the visible region and the $Co^{III}Mo^{IV} \leftrightarrows Co^{II}Mo^{V}$ spin equilibrium strongly dominated by the $Co^{III}Mo^{IV}$ form. We show a gentle thermal treatment of diamagnetic compounds **1**−**4** leading to the dehydrated forms **1a**−**4a**, which reveal a significant increase of paramagnetic contribution (from 0.5 to 2% to 30−40%). The rehydration allows to recover the diamagnetic phases **1b**−**4b** of compositions and properties similar to those of **1**−**4**. The irradiation of the dehydrated form **2a** within the MMCT band in the Superconducting Quantum Interference Device (SQUID) cavity at T = 10 K causes further increase of the $Co^{II}Mo^{V}$ contribution giving the metastable phase annealed back to the **2a** phase after heating above T = 290 K. The IR, electron paramagnetic resonance (EPR), and X-ray photoelectron spectroscopy (XPS) spectroscopic data along with the magnetic data are interpreted in terms of strong modification of the $Co^{III}Mo^{IV} \leftrightarrows Co^{II}Mo^{V}$ equilibrium occurring in these systems.

Introduction

Coordination compounds gained much attention in the search of new switchable or tunable materials. A particular interest is paid to cyano-bridged bimetallic systems, where both metallic centers participate in structural and electrochemical modifications upon the external stimuli.[1−3] As the result of dynamic research activity in this field, several pairs of cyano-bridged compounds of 3d ions revealed a potential to form $Co^{HS,II}$-$Fe^{LS,III} \leftrightarrows Co^{LS,III}$-$Fe^{LS,II}$,[4−8] $Fe^{LS,II}$-$Mn^{HS,III} \leftrightarrows Fe^{LS,III}$-$Mn^{HS,II}$,[9−12] or $(O_h)Co^{II}-Cr^{III} \leftrightarrows (T_d)Co^{II}-Cr^{III}$ [13] equilibria in the solid state. Recently similar phenomena in

*To whom correspondence should be addressed.E-mail: mathon@icmcb-bordeaux.cnrs.fr (C.M.), barbara.sieklucka@uj.edu.pl (B.S.). Fax: +33 5 40 00 26 49 (C.M.), +48 12 634 05 15 (B.S.).

(1) Sato, O.; Tao, J.; Zhang, Y.-Zh. *Angew. Chem., Int. Ed.* **2007**, *46*, 2152–2187.
(2) Real, J. A.; Gaspar, A. B.; Muñoz, M. C. *Dalton Trans.* **2005**, 2062–2079.
(3) Bleuzen, A.; Marvaud, V.; Mathonière, C.; Sieklucka, B.; Verdaguer, M. *Inorg. Chem.* **2009**, *48*, 3453–3466.
(4) Bleuzen, A.; Lomenech, C.; Escax, V.; Villain, F.; Varret, F.; Cartier dit Moulin, C.; Verdaguer, M. *J. Am. Chem. Soc.* **2000**, *122*, 6648–6652.
(5) Escax, V.; Bleuzen, A.; Cartier dit Moulin, C.; Villain, F.; Goujon, A.; Varret, F.; Verdaguer, M. *J. Am. Chem. Soc.* **2001**, *123*, 12536–12543.
(6) Goujon, A.; Varret, F.; Escax, V.; Bleuzen, A.; Verdaguer, M. *Polyhedron* **2001**, *20*, 1347–1354.
(7) Pejakovic, D. A.; Manson, J. L.; Miller, J. S.; Epstein, A. J. *J. Appl. Phys.* **2000**, *87*, 6028–6030.
(8) Shimamoto, N.; Ohkoshi, S.; Sato, O.; Hashimoto, K. *Inorg. Chem.* **2002**, *41*, 678–684.
(9) Moritomo, Y.; Hanawa, M.; Ohishi, Y.; Kato, K.; Takata, M.; Kuriki, A.; Nishibor, E.; Sakata, M.; Ohkoshi, S.; Tokoro, H.; Hashimoto, K. *Phys. Rev. B* **2003**, *68*, 4106–4112.
(10) Ohkoshi, S.; Matsuda, T.; Tokoro, H.; Hashimoto, K. *Chem. Mater.* **2005**, *17*, 81–84.
(11) Ohkoshi, S.; Tokoro, H.; Hashimoto, K. *Coord. Chem. Rev.* **2005**, *249*, 1830–1840.
(12) Tokoro, H.; Ohkoshi, S.; Matsuda, T.; Hashimoto, K. *Inorg. Chem.* **2004**, *43*, 5231–5236.
(13) Sato, Y.; Ohkoshi, S.; Arai, K.; Tozawa, M.; Hashimoto, K. *J. Am. Chem. Soc.* **2003**, *125*, 14590–14595.

Published on Web 02/10/2010

mixed 3d-4d or 4d-5d systems were also observed. For example, the photocontrol of the magnetization in magnetically ordered $Cu^{II}Mo^{V}$ 3D phases[14−16] or high-spin clusters[17,18] can be interpreted by a light-induced metal-to-metal charge transfer (MMCT) between paramagnetic $\{Cu^{II}(S = {}^1/_2)$-$[Mo^{IV}(CN)_8](S=0)$-$Cu^{II}(S=1/2)\}$ and magnetically coupled $\{Cu^{II}(S={}^1/_2)$-$[Mo^{V}(CN)_8](S={}^1/_2)$-$Cu^{I}(S=0)\}$ states. Analogously to CoFe Prussian-Blue analogues, the thermal charge-transfer-induced-spin-transition (CTIST) with the hysteretic character was observed between high-temperature $\{Co^{HS,II}$-$[W^{V}(CN)_8]\}$ phase and low-temperature $\{Co^{LS,III}$-$[W^{IV}(CN)_8]\}$ phases. The light-induced-excited-spin-state-trapping (LIESST) at low temperatures allowed to obtain the metastable magnetically ordered $\{Co^{HS,II}$-$[W^{V}(CN)_8]\}$ phase with a Curie temperature around 35 K, relaxing thermally to the original $\{Co^{LS,III}$-$[W^{IV}(CN)_8]\}$ state around 120 K.[19,20]

Focusing on the design of novel materials we decided to explore further the potential of $Co^{III/II}$ complexes in the construction of bimetallic systems with tunable properties. Actually, relatively low number of cobalt-octacyanometalate systems were presented to date. The reported systems include: 0-D clusters $\{Co^{II}{}_9[W^{V}(CN)_8]_6\cdot(CH_3OH)_{24}\}\cdot 19H_2O$, $\{Co^{II}{}_9[Mo^{V}(CN)_8]_6\cdot(CH_3OH)_{24}\}\cdot 4CH_3OH\cdot 16H_2O$,[21] $[\{Co^{II}(phen)_2\}_6\{W^{IV}(CN)_8\}_2Cl_2]Cl_2$,[22] 1-D chains $\{[Co^{II}{}_3(DMF)_{12}][W^{V}(CN)_8]_2\}_\infty$,[23] 2-D layers $Cs[\{Co^{II}(3\text{-cyanopyridine})_2\}$-$\{W^{V}(CN)_8\}]\cdot H_2O$,[19] $\{Co^{II}{}_3(H_2O)_6(pyz)_3[W^{V}(CN)_8]_2\}\cdot 3.5H_2O$, $\{Co^{II}{}_3(H_2O)_4(4,4'\text{-bpy})_3[W^{V}(CN)_8]_2\}\cdot 1.5(4,4'\text{-bpy})\cdot 6H_2O$[24] and 3-D networks $[W^{IV}\{(\mu\text{-CN})_4Co^{II}(H_2O)_2\}_2\cdot 4H_2O]_n$, $[\{W^{V}(CN)_2\}_2\{(\mu\text{-CN})_4Co^{II}(H_2O)_2\}_3\cdot 4H_2O]_n$,[25] $[Co^{II}(H_2O)_2]_2[Mo^{IV}(CN)_8]\cdot 4H_2O$,[26] $Co^{II}{}_3[W^{V}(CN)_8]_2(\text{pyrimidine})_4\cdot 6H_2O$.[20,27]

Some of these CN-bridged systems exhibit MMCT bands[20,24,27] which were successfully exploited for the studies of the photomagnetic effect.[20,27] Analogous MMCT bands, recognized as Outer-Sphere (Ion-Pair) Charge Transfer (OSCT, IPCT) were observed in several ionic compounds.[28−36]

In this work we examine for the first time the properties of the bimetallic ionic pairs of $\{Co^{III}$-$[Mo^{IV}(CN)_8]\}$, exhibiting an IPCT band in the visible part of electronic spectra. The synthesis and the X-ray structures, as well as the thermal, optical, and magnetic properties, of the ionic compounds of general formula: $M^{I}[Co(bpy)_3][Mo(CN)_8]\cdot nH_2O$ (M^{I} = Li (**1**), K (**2**), Rb (**3**), Cs (**4**); n = 7−8) are presented.

Experimental Section

Materials and Methods. All chemicals and solvents of reagent grade were purchased from Aldrich Chemicals Co. and used as received. $K_4[Mo(CN)_8]\cdot 2H_2O$ and $[Co(bpy)_3]Cl_2$ were prepared according to the literature procedures.[37,38] $[Co(bpy)_3]Cl_3$ was prepared by oxidation of $[Co(bpy)_3]Cl_2$ with hydrogen peroxide in HCl, evaporation, and recrystallization from water. The solutions of $M_4[Mo(CN)_8]$ (M = Li, Rb, Cs) were prepared by precipitation of $Cd_2[Mo(CN)_8]\cdot nH_2O$ followed by double exchange reaction with hydroxide of appropriate alkali metal and filtration of the precipitated $Cd(OH)_2$. If not stated otherwise, all measurements were carried out for ground samples of monocrystalline compounds. Elemental analyses were performed on a EuroEA EuroVector elemental analyzer. Reflectance electronic spectra of the solid phases were recorded on a Perkin-Elmer Lambda 35 UV−vis spectrometer equipped with a 50 mm integrating sphere in the 190−1100 nm wavelength range. Infrared spectra were measured between 4000 and 400 cm^{-1} on a Bruker EQUINOX 55 spectrometer in KBr pellets. X-ray photoelectron spectroscopy (XPS) spectra were recorded using a 220i-XL ESCALAB from VG. Powder samples were pressed onto indium foils and put under UHV (10^{-8} Pa). The non-monochromatized Mg X-ray source was used at 200 W, as well as a flood gun to compensate for the nonconductive samples. The spectra were calibrated in relation to the C1s binding energy (284.6 eV), which was applied as an internal standard. Fitting of the high-resolution spectra was provided through the AVANTAGE program from VG. The X-band electron paramagnetic resonance (EPR) measurements at room temperature and at 77 K were recorded with a Bruker ELEXSYS-E500 spectrometer. For quantitative determination of spin concentration in the samples, the standards based on $VOSO_4$ diluted with K_2SO_4 were used.[39] The EPR spectra of the investigated sample and the standard were measured with the same spectrometer settings. Then, the spectra were integrated twice, and areas under the adsorption curves were determined. The number of the spin was calculated using following formula: $N_x = (I_p/I_s)N_s$, where I_p is the sample signal intensity, I_s is the standard signal intensity, N_s is the number of the spin in the standard. The X-band EPR measurements at 4 K were performed using a Bruker EXELIS spectrometer equipped with helium cryostat. Thermogravimetric data in the temperature range 25−400 °C were collected on a Mettler

(14) Catala, L.; Mathonière, C.; Gloter, A.; Stephan, O.; Gacoin, Th.; Boilot, J. P.; Mallah, T. *Chem. Commun.* **2005**, 746–748.
(15) Ohkoshi, S.; Tokoro, H.; Hozumi, T.; Zhang, Y.; Hashimoto, K.; Mathonière, C.; Bord, I.; Rombaut, G.; Verelst, M.; Cartier dit Moulin, Ch.; Villain, F. *J. Am. Chem. Soc.* **2006**, *128*, 270–277.
(16) Hozumi, T.; Hashimoto, K.; Ohkoshi, S. *J. Am. Chem. Soc.* **2005**, *127*, 3864–3869.
(17) Herrera, J. M.; Marvaud, V.; Verdaguer, M.; Marrot, J.; Kalisz, M.; Mathoniere, C. *Angew. Chem., Int. Ed.* **2004**, *43*, 5468–5471.
(18) Long, J.; Chamoreau, L. -M.; Mathonière, C.; Marvaud, V. *Inorg. Chem.* **2009**, *48*, 22–24.
(19) Arimoto, Y.; Ohkoshi, S.; Zhong, Zh. J.; Seino, H.; Mizobe, Y.; Hashimoto, K. *J. Am. Chem. Soc.* **2003**, *125*, 9240–9241.
(20) Ohkoshi, S.; Hamada, Y.; Matsuda, T.; Tsunobuchi, Y.; Tokoro, H. *Chem. Mater.* **2008**, *20*, 3048–3054.
(21) Song, Y.; Zhang, P.; Ren, X. -M.; Shen, X. -F.; Li, Y. -Z.; You, X. -Z. *J. Am. Chem. Soc.* **2005**, *127*, 3708–3709.
(22) Venkatakrishnan, T. S.; Imaz, I.; Sutter, J.-P. *Inorg. Chim. Acta* **2008**, 3710–3713.
(23) Li, D.; Zheng, L.; Zhang, Y.; Huang, J.; Gao, S.; Tang, W. *Inorg. Chem.* **2003**, *42*, 6123–6129.
(24) Podgajny, R.; Bałanda, M.; Sikora, M.; Borowiec, M.; Spałek, L.; Kapusta, Cz.; Sieklucka, B. *Dalton Trans.* **2006**, 2801–2809.
(25) Herrera, J. M.; Bleuzen, A.; Dromzée, Y.; Julve, M.; Lloret, F.; Verdaguer, M. *Inorg. Chem.* **2003**, *42*, 7052–7059.
(26) Willemin, S.; Larionova, J.; Clérac, R.; Donnadieu, B.; Henner, B.; Le Goff, X. F.; Guérin, C. *Eur. J. Inorg. Chem.* **2003**, 1866–1872.
(27) Ohkoshi, S.; Ikeda, S.; Hozumi, T.; Kashiwagi, T.; Hashimoto, K. *J. Am. Chem. Soc.* **2006**, *128*, 5320–5321.
(28) Vogler, A.; Osman, A. H.; Kunkely, H. *Coord. Chem. Rev.* **1985**, *64*, 159.
(29) Billing, R.; Vogler, A. *J. Photochem. Photobiol., A* **1997**, *103*, 239–247.
(30) Curtis, J. C.; Meyer, T. J. *Inorg. Chem.* **1982**, *21*, 1562–1571.
(31) Curtis, J. C.; Sullivan, B. P.; Meyer, T. J. *Inorg. Chem.* **1980**, *19*, 3833–3839.
(32) Podgajny, R.; Sieklucka, B.; Łasocha, W. *J. Chem. Soc., Dalton Trans.* **2000**, 1799–1803.
(33) Nowicka, B.; Samotus, A. *J. Chem. Soc., Dalton Trans.* **1998**, 1021–1024.
(34) Siekluska, B. *J. Chem. Soc., Dalton Trans.* **1997**, 869–872.
(35) Alcock, N. W.; Samotus, A.; Szklarzewicz, J. *J. Chem. Soc., Dalton Trans.* **1993**, 885–889.
(36) Toma, H. E. *J. Chem. Soc., Dalton Trans.* **1980**, 471–475.
(37) Leipoldt, J. G.; Bok, L. D. C.; Cilliers, P. J. *Z. Anorg. Allg. Chem.* **1974**, *407*, 350–352.
(38) Burstall, F. H.; Nyholm, R. S. *J. Chem. Soc.* **1952**, 3570.
(39) Dyrek, K.; Rokosz, A.; Madej, A.; Bedzińska, E. *Appl. Magn. Reson.* **1996**, *10*, 319–338.

Toledo TGA/SDTA 851e microthermogravimeter equipped with QMS (Quadrupole Mass Spectrometer) Thermostar GSD 300 T Balzers at heating rate of 5 °C·min^{-1} in Ar atmosphere. Magnetic susceptibility measurements were performed for powder samples using a Superconducting Quantum Interference Device (SQUID) Quantum Design magnetometer. Diamagnetic corrections were calculated on the basis of Pascal tables. The sample in the EPR experiment was irradiated with laser light λ = 620 nm of power about 20 mW/cm^2. The photomagnetic experiments were performed with an Ar−Kr laser (Spectra Physics Beamlok) coupled through an optical fiber directed into the magnetometer cavity. A 1.3 mg portion for **2** of a finely ground powdered sample was deposited in a formed SQUID straw as a thin layer and maintained at about 4 cm from the optical fiber. Data in the dark have been systematically subtracted at each temperature from the data after irradiation without any type of correction. The obtained difference was simply added to the direct current (dc) measurements obtained with the standard SQUID setup to plot the final data after irradiation. The effective power of the light received by the sample was measured at 20 mW/cm^2.

General Synthesis. The aqueous solution of $[Co(bpy)_3]Cl_3 \cdot 4H_2O$ (0.14 g, 0.2 mmol, 3 mL) was added to the aqueous solution of $M^I_4[Mo(CN)_8]$ containing M^ICl. To the resulting brown solution CH_3CN was added, and the color turned green. After 1 day, the solid product was washed with small amount of ice-cold water and air-dried.

Synthesis of Li[Co(bpy)$_3$][Mo(CN)$_8$]·8H$_2$O (1). $Li_4[Mo(CN)_8]$: 2.38 mL, c = 0.084 mol·L^{-1}, 0.2 mmol; LiCl: 0.1 g; CH_3CN: 2 mL; Product: brown needles. Yield: 62 mg, 32%. Found: C, 46.58%; H, 3.83%; N, 19.99%. Calcd for $C_{38}H_{40}CoLiMoN_{14}O_8$: C, 46.45%; H, 4.1%; N, 19.96%. Selected FT-IR data [ν_{CN}/cm^{-1}]: 2118 (vs), 2105 (vs), 2095 (vs).

Synthesis of K[Co(bpy)$_3$][Mo(CN)$_8$]·8H$_2$O (2). $K_4[Mo(CN)_8]$: 4 mL, c = 0.05 mol·L^{-1}, 0.2 mmol; KCl: 0.07 g; CH_3CN: 4 mL; Product: brown plates. Yield: 75 mg, 37%. Found: C, 45.14%; H, 4.01%; N, 19.38%. Calcd for $C_{38}H_{40}CoKMoN_{14}O_8$: C, 44.98%; H, 3.97%; N, 19.32%. Selected FT-IR data [ν_{CN}/cm^{-1}]: 2118 (vs), 2095 (vs).

Synthesis of Rb[Co(bpy)$_3$][Mo(CN)$_8$]·8H$_2$O (3). $Rb_4[Mo(CN)_8]$: 4.26 mL, c = 0.047 mol·L^{-1}, 0.2 mmol; RbCl: 0.11 g; CH_3CN: 3 mL; Product: brown needles. Yield: 100 mg, 47%. Found: C, 43.21%; H, 3.74%; N, 18.5%. Calcd for $C_{38}H_{40}CoMoN_{14}O_8Rb$: C, 43.01%; H, 3.8%; N, 18.48%. Selected FT-IR data [ν_{CN}/cm^{-1}]: 2119 (vs), 2096 (vs).

Synthesis of Cs[Co(bpy)$_3$][Mo(CN)$_8$]·7.5H$_2$O (4). $Cs_4[Mo(CN)_8]$: 2.66 mL, c = 0.075 mol·L^{-1}, 0.2 mmol; CsCl: 0.15 g; CH_3CN: 2 mL; Product: brown plates. Yield: 89 mg, 40%. Found: C, 41.85%; H, 3.7%; N, 17.91%. Calcd for $C_{38}H_{39}CoCsMoN_{14}O_{7.5}$: C, 41.51%; H, 3.57%; N, 17.83%. Selected FT-IR data [ν_{CN}/cm^{-1}]: 2118 (vs), 2097 (vs).

Dehydrated compounds $M^I[Co(bpy)_3][Mo(CN)_8]\cdot nH_2O$ (M^I = Li (**1a**), K (**2a**), Rb (**3a**), Cs (**4a**); n < 2) were obtained by heating powder samples of **1**−**4** in an oven at 355 K for 24 h and stored in anhydrous conditions.

X-ray Crystallography Studies. Single-crystal X-ray data for compounds **2**−**4** were collected at liquid nitrogen temperature on a Nonius KappaCCD diffractometer with graphite monochromated Mo−K$_\alpha$ radiation (λ = 0.71070 Å). X-ray crystallographic data for **1** were not measured because of the poor quality of the crystals. For cell refinement and data reduction the DENZO-SCALEPACK[40] program package was used. The structure of **2**−**4** was solved by direct methods (SIR97[41]) and refined by full-matrix least-squares on F^2 using the program SHELXL-97.[42] However, it was impossible to completely refine the structure of **4** because of considerable disorder in this system. Crystallographic data and collection parameters for **2**−**4** are listed in Table 1.

Table 1. Crystallographic Data for **2**−**4**

	2	**3**	**4**
formula	$C_{38}H_{40}CoKMoN_{14}O_8$	$C_{38}H_{40}CoMoN_{14}O_8Rb$	$C_{38}H_{39}CoCsMoN_{14}O_{7.5}$
FW	1014.8	1061.2	1100.62
crystal system	monoclinic	monoclinic	monoclinic
space group	$P2_1/c$	$P2_1/c$	$P2_1$
a [Å]	16.7580(2)	16.6390(3)	16.7070(3)
b [Å]	13.8940(2)	13.8060(2)	13.7610(2)
c [Å]	19.3940(4)	19.4510(3)	19.5690(4)
$\alpha = \gamma$ [deg]	90	90	90
β [deg]	106.818(10)	107.2180(10)	107.3790(10)
V [Å^3]	4322.47(12)	4268.00(12)	4293.63(13)
Z	4	4	4
μ	0.838	1.884	1.581
parameters	615	649	
R1	0.0480	0.0543	
wR2	0.0850	0.0843	
gof	1.044	1.048	

X-ray powder diffraction measurements were performed on Philips X'Pert Pro diffractometer with a Bragg−Brentano geometry using Cu K$_\alpha$ radiation (λ = 1.54178 Å) at 298 K in the 3.5−40° 2θ angle range.

Results

Crystal Structures. Crystallographic studies on compounds **2**, **3**, and **4** have shown that they are all isomorphous. The comparison of structural parameters for compounds **2**−**4** is presented in Table 1. Selected interatomic distances and angles for compound **2** and **3** are listed in Tables 2 and 3, respectively. The molecular structure of **2** consists of $[Co(bpy)_3]^{3+}$ and $[Mo(CN)_8]^{4-}$ complexes, K^+ ions, and water molecules. The asymmetric unit and the view on *ab* crystallographic plane of compound **2** are shown in Figures 1 and 2, respectively. Coordination sphere analyses for Mo and Co centers using the SHAPE[43−46] program were performed. The Continuous Shape Measures (CShM) and other shape parameters are collected in Table 4. $[Mo(CN)_8]^{4-}$ ions have an intermediate geometry between a dodecahedron and a square antiprism. Average bond lengths Mo−C (2.16 Å) and C−N (1.15 Å) and angles Mo−C−N (177°) are in the range typical for octacyanometalates(IV).[47,48] Potassium ions are located between the two neighboring $[Mo(CN)_8]^{4-}$ ions forming one end-on K···N−C−Mo linkage with one Mo center (K···N distance 2.8 Å, K···Mo distance 5.9 Å, K···N−C angle 150.6°) and

(40) Otwinowski, Z.; Minor, W., *Macromolecular Crystallography*, Part A; Carter, C. W., Jr., Sweet, R. M., Eds.; Academic Press: New York, 1997; Methods in Enzymology, Vol. *276*, pp 307−326.
(41) Altomare, A.; Burla, M. C.; Camalli, M.; Cascarano, G. L.; Giacovazzo, C.; Guagliardi, A.; Moliterni, A. G. G.; Polidori, G.; Spagna, R. *J. Appl. Crystallogr.* **1999**, *32*, 115–119.
(42) Sheldrick, G. M. *Acta Crystallogr.* **2008**, *A64*, 112–122.
(43) Alvarez, S.; Alemany, P.; Casanova, D.; Cirera, J.; Llunell, M.; Avnir, D. *Coord. Chem. Rev.* **2005**, *249*, 1693–1708.
(44) Casanova, D.; Cirera, J.; Llunell, M.; Alemany, P.; Avnir, D.; Alvarez, S. *J. Am. Chem. Soc.* **2004**, *126*, 1755–1763.
(45) Casanova, D.; Llunell, M.; Alemany, P.; Alvarez, S. *Chem.—Eur. J.* **2005**, *11*, 1479–1494.
(46) Llunell, M.; Casanova, D.; Cirera, J.; Bofill, J. M.; Alemany, P.; Alvarez, S.; Pinsky, M.; Anvir, D. *SHAPE*, v. 1.1b.; University of Barcelona: Barcelona, Spain, 2005.
(47) Sieklucka, B.; Podgajny, R.; Przychodzeń, P.; Korzeniak, T. *Coord. Chem. Rev.* **2005**, *249*, 2203–2221.
(48) Przychodzeń, P.; Korzeniak, T.; Podgajny, R.; Sieklucka, B. *Coord. Chem. Rev.* **2006**, *250*, 2234–2260.

Table 2. Selected Bond Lengths (in angstroms) and Angles (in degrees) for **2**

Mo−C01	2.171(3)	C01−N01	1.149(4)
Mo−C02	2.164(3)	C02−N02	1.153(4)
Mo−C03	2.162(4)	C03−N03	1.154(5)
Mo−C04	2.164(3)	C04−N04	1.153(4)
Mo−C05	2.160(4)	C05−N05	1.150(5)
Mo−C06	2.179(4)	C06−N06	1.143(4)
Mo−C07	2.150(3)	C07−N07	1.152(4)
Mo−C08	2.158(3)	C08−N08	1.152(4)
C06−Mo−C08	69.38(12)	C03−Mo−C05	72.15(14)
C06−Mo−C07	76.99(13)	C03−Mo−C01	76.02(12)
C07−Mo−C08	86.22(13)	C03−Mo−C02	76.48(13)
C01−Mo−C02	73.43(11)	C03−Mo−C08	145.92(12)
Co−N101	1.937(2)	N101−C106	1.357(4)
Co−N112	1.933(2)	C106−C107	1.460(5)
Co−N201	1.937(2)	C107−N112	1.359(4)
Co−N212	1.933(2)	N101−C102	1.339(4)
Co−N301	1.937(2)	C102−C103	1.369(5)
Co−N312	1.942(2)	C103−C104	1.366(6)
N101−Co−N112	83.55(11)	N101−Co−N301	87.87(10)
N201−Co−N212	83.06(10)	N101−Co−N201	95.27(10)
N301−Co−N312	83.07(10)	N101−Co−N212	177.32(10)
K−C06	3.234(3)		
K−N06	3.016(3)	K−N03	2.800(4)
K−C07	3.388(4)	K−O1	2.739(5)
K−N07	3.277(5)	K−O2A	2.698(8)
K−C08	3.309(3)	K−O2B	2.843(10)
K−N08	3.119(3)		

Table 3. Selected Bond Lengths (in angstroms) and Angles (in degrees) for **3**

Mo−C1	2.166(4)	C1−N1	1.156(5)
Mo−C2	2.172(4)	C2−N2	1.150(5)
Mo−C3	2.159(4)	C3−N3	1.156(5)
Mo−C4	2.161(4)	C4−N4	1.159(5)
Mo−C5	2.158(4)	C5−N5	1.153(5)
Mo−C6	2.174(4)	C6−N6	1.161(5)
Mo−C7	2.153(4)	C7−N7	1.154(5)
Mo−C8	2.159(4)	C8−N8	1.163(5)
C6−Mo−C8	69.88(14)	C3−Mo−C5	72.61(16)
C6−Mo−C7	77.12(14)	C3−Mo−C1	75.92(13)
C7−Mo−C8	85.77(13)	C3−Mo−C2	75.75(13)
C1−Mo−C2	73.79(13)	C3−Mo−C8	145.24(14)
Co−N101	1.932(3)	N101−C106	1.361(5)
Co−N112	1.931(3)	C106−C107	1.462(5)
Co−N201	1.933(3)	C107−N112	1.362(5)
Co−N212	1.924(3)	N101−C102	1.352(5)
Co−N301	1.939(3)	C102−C103	1.383(5)
Co−N312	1.932(3)	C103−C104	1.374(6)
N101−Co−N112	83.51(13)	N101−Co−N301	88.37(12)
N201−Co−N212	83.00(12)	N101−Co−N201	95.10(12)
N301−Co−N312	83.17(12)	N101−Co−N212	177.07(13)
RbA−C6	3.347(4)	RbA−N3	2.900(3)
RbA−N6	3.147(5)	RbA−O1A	2.834(11)
RbA−C7	3.378(4)	RbA−O1B	2.84(3)
RbA−N7	3.232(4)	RbA−O2A	2.957(5)
RbA−C8	3.388(4)	RbA−O2B	2.844(9)
RbA−N8	3.214(4)		

three side-on contacts with cyano ligands of another Mo center (av. K···N distance 3.1 Å, av. K···C distance 3.3 Å, K···Mo distance 4.4 Å, K···N−C angles 85 to 91°). Such chain-like arrangement expands along the *c* direction. There are also two water molecules completing the coordination sphere of the K^+ ion. One of these molecules can occupy one of two alternative positions (O2A and O2B in occupancy ratio 46:54) what indicates

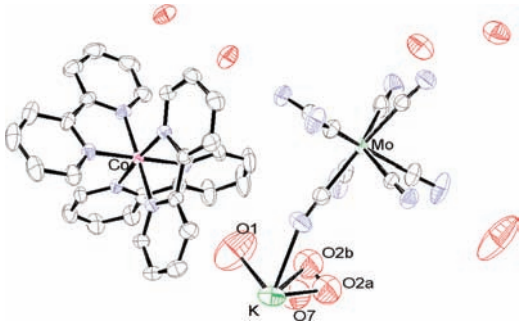

Figure 1. Asymmetric unit of **2**. Hydrogen atoms are omitted for clarity. Ellipsoids at 50%.

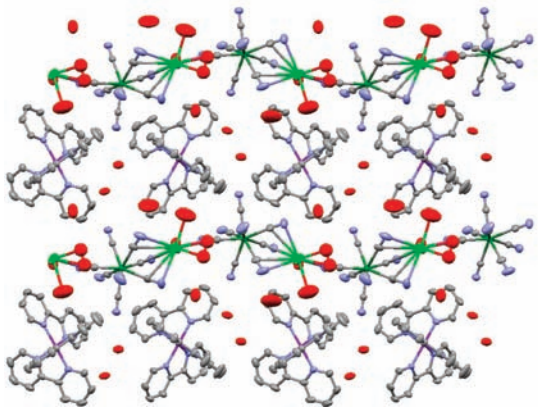

Figure 2. Crystal structure of **2**. View on *bc* plane. Hydrogen atoms are omitted for clarity. Ellipsoids at 50%.

small disorder in the crystal lattice. In the 3D architecture the chains of $[Mo(CN)_8]^{4-}$ and K^+ ions are separated by columns of $[Co(bpy)_3]^{3+}$ ions which have D_3 geometry (trigonally distorted octahedron) with its trigonal axis along the *c* direction. Average Co−N bond lengths (1.9 Å) and N−Co−N angles (83° for biting angle, 92° for N atoms of two different bpy ligands) are typical for Co-bpy complexes and indicate the presence of Co^{III}_{LS} species.[49,50] The shortest Co···Mo distance equals 7.25 Å. All cyano ligands are pointed toward spaces between $[Co(bpy)_3]^{3+}$ moieties.

The crystal structure of **3** exhibits significant disorder; rubidium ions can occupy one of two alternative positions (RbA and RbB in occupancy ratio 78:22) as well as two water molecules (O1A and O1B in occupancy ratio 77:23 and O2A and O2B in occupancy ratio 65:35).

Thermogravimetric Studies. Thermogravimetric analysis (TGA) results for **2** presented in the Supporting Information, Figure S1 show the almost complete loss of water molecules during heating up to 380 K (for **2** loss of $8H_2O$ molecules, 14.2% of mass, experimental: 12%). This loss is accompanied by a color change from brown to dark green (for single crystals) or dark gray (for powder). Similar results were obtained for compounds **1**, **3**, and **4**. Powder X-ray diffraction proved that the resulting substances (named hereafter **1a**−**4a**) are amorphous. After return to ambient conditions, the resulting materials

(49) Bhat, Gh. R.; Dubey, K. P.; Segal, B.; Pierpont, C. G. *Acta Crystallogr., Sect. C* **1988**, *44*, 999–1001.
(50) Reimann, C. W.; Zocchi, M.; Mighell, A. D.; Santoro, A. *Acta Crystallogr., Sect. B* **1971**, *27*, 2211–2218.

Table 4. Continuous Shape Measures (CShM), Minimal Distortion Path Deviation Functions (Δ_i) and the Angular Path Fractions (ϕ) for Co and Mo Centers in **2**[43−46]

center	coordination number	reference polyhedron	CShM	θ	Δ_i	ϕ
Co	6	Octahedron	0.382	24.149	0.110	14.7%
		Trigonal prism	15.590			96.3%
Mo	8	Dodecahedron	0.692	9.716	0.101	49.1%
		Square antiprism	1.067			61.0%

undergo a fast rehydration process producing amorphous materials **1b**−**4b** of original composition $M^I[Co(bpy)_3][Mo(CN)_8]\cdot nH_2O$ (M^I = Li, n = 8 (**1**), M^I = K, n = 8 (**2**), M^I = Rb, n = 8 (**3**), M^I = Cs, n = 7.5 (**4**)).

UV−vis Spectroscopy. UV−vis spectra of compounds **1**−**4** are very similar to each other; therefore we exemplify the electronic spectra in the solution and in the solid state for $K[Co(bpy)_3][Mo(CN)_8]\cdot 8H_2O$ (**2**) (Supporting Information, Figure S2). Compared to the UV−vis spectra of the precursor complexes, $[Co(bpy)_3]Cl_3$ and $K_4[Mo(CN)_8]$, the compound **2** exhibits a net increased absorption in the range 10000−20000 cm^{-1} (500−1000 nm) with the maximum at about 15385 cm^{-1} (650 nm) which can be attributed to a MMCT band from Mo^{IV} to Co^{III}. The electron delocalization parameter (α) and coupling parameter (H_{if}) in terms of the Hush theory[51,52] were calculated based on spectral parameters of the MMCT band measured in solution. Obtained values ($\alpha^2 = 8.6 \times 10^{-4}$, H_{if} = 463 cm^{-1}) indicate weak-to-moderate coupling between Co(III) and Mo(IV). This assignment is consistent with the redox potentials of the $[Mo(CN)_8]^{3-/4-}$ and $[Co(bpy)_3]^{3+/2+}$ complexes ($E_{Mo^{V/IV}}{}^o$ = 0.78 V vs NHE,[53] $E_{Co^{III/II}}{}^o$ = 0.61 V vs NHE[54]) which classifies compounds **1**−**4** in the class II of the Robin−Day classification.[55,56] UV−vis spectra of **1a**−**4a** show high absorption in the whole measured range with no clear evidence of maxima, and it was impossible to analyze further by deconvolution methods.

IR Spectroscopy. FT-IR spectra of **1**−**4** in the ν(CN) region exhibit sharp bands around 2118 cm^{-1} (vs) and 2095 cm^{-1} (vs), confirming the presence of terminal CN^- ligands in the $[Mo^{IV}(CN)_8]^{4-}$ moieties (Supporting Information, Figure S3).[47,48] In dehydrated **1a**−**4a** and rehydrated **1b**−**4b** compounds the two peaks disappear to give a single broader component shifted to higher energy at 2103 cm^{-1}. Moreover, a new band at 2152 cm^{-1} (m) appears (Supporting Information, Figure S4). The broadening of the bands is attributed to the collapse of the crystal structure. The shift to higher energy and the appearance of the new band may be attributed to the removal of H_2O molecules and the structural change involving K···N−C−Mo linkages in both, dehydrated and rehydrated phases. In the dehydrated phases the presence of the $[Mo^V(CN)_8]^{3-}$ may give additional contribution to the 2152 cm^{-1} band.[47,48]

XPS Studies. To confirm the oxidation states of metal centers in compounds **1a**−**4a**, XPS measurements were performed. The XPS spectra confirm qualitative composition of the samples, including the presence of respective

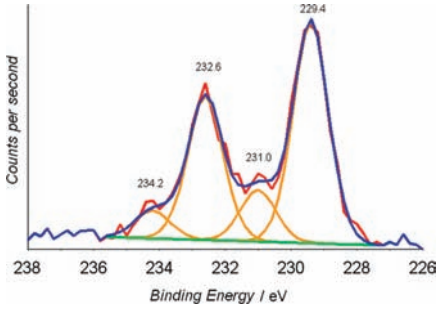

Figure 3. XPS spectrum of **2a** in the Mo 3d region. The signal (red) and best fit (blue) after background subtraction (green) is presented.

alkali cations. In the 3d Mo region, the compound **2a** shows 4 peaks (Figure 3). The split of the Mo 3d peaks observed with the binding energies 229.4, 231.0, 232.6, and 234.2 eV can be attributed respectively to Mo^{IV} $3d_{5/2}$, Mo^V $3d_{5/2}$, Mo^{IV} $3d_{3/2}$, and Mo^V $3d_{3/2}$[57] in agreement with the fitting curves. The signal ratio calculated as the ratio of the area of the peaks attributed to Mo^{IV} and Mo^V, respectively, gives the amount of Mo^V equal about 18% for compound **2a**. Co 2p signals, broader than usual, suggest two oxidation states for cobalt ion, but the fitting of the peaks does not give a reasonable analysis. Finally, results for **1a**, **3a**, and **4a** are similar (amount of Mo^V equal ca. 16%, 15%, 17%, respectively; Supporting Information, Figures S5−S7).

EPR Studies. The EPR measurements at 77 K give very similar results for all compounds **1**−**4** (Figure 4). As an example, the spectra of **2** exhibit a weak but distinct signal with a low g tensor symmetry (g_1 = 2.002, g_2 = 2.001, g_3 = 1.989, Figure 5). We attribute this signal to the paramagnetic Mo^V centers. It is characterized by hyperfine structure (HFS; A1 = 53.2 mT, A2 = 18.8 mT, A3 = 24.5 mT for **2**) resulted from the natural abundance of magnetically active molybdenum isotopes: ^{95}Mo (I = 5/2, 15.72%) and ^{97}Mo (I = 5/2, 9.46%). Estimation of the amount of Mo^V centers was performed using quantitative EPR measurements, and the results are presented in Table 5. For samples **1a**−**4a** the molybdenum signal is much stronger, with visible hyperfine structure (Supporting Information, Figure S8). The symmetry of the g-tensor is higher, probably because of the amorphous character of the samples. The crude estimation (because of rapid rehydration) of the amount of Mo^V centers for **2a** indicates the presence of at least 20% of Mo^V per all Mo centers (Table 5).

To observe the X-band EPR signal of high spin cobalt complexes, liquid helium temperature is often required because of the very fast spin−lattice relaxation at room temperature.[58] For **2a** the signal for $[Co^{II}(bpy)_3]^{2+}$ is

(51) Hush, N. S. *J. Electroanal. Chem.* **1999**, *470*, 170.
(52) Hush, N. S. *Trans. Faraday Soc.* **1961**, *57*, 557.
(53) Samotus, A.; Szklarzewicz, J. *Coord. Chem. Rev.* **1993**, *125*, 63–74.
(54) Farina, R.; Wilkins, R. G. *Inorg. Chem.* **1968**, *7*, 514–518.
(55) Robin, M. B.; Day, P. *Adv. Inorg. Chem. Radiochem.* **1967**, *10*, 247–422.
(56) Macpherson, B. P.; Bernhardt, P. V.; Hauser, A.; Pages, S.; Vauthey, E. *Inorg. Chem.* **2005**, *44*, 5530–5536.
(57) Mathonière, C.; Podgajny, R.; Guionneau, P.; Labrugere, C.; Sieklucka, B. *Chem. Mater.* **2005**, *17*, 442–449.
(58) Mabbs, F. E.; Collison, D. *Electron Paramagnetic Resonance of d Transition Metal Ions*; Elsevier: Amsterdam, 1992

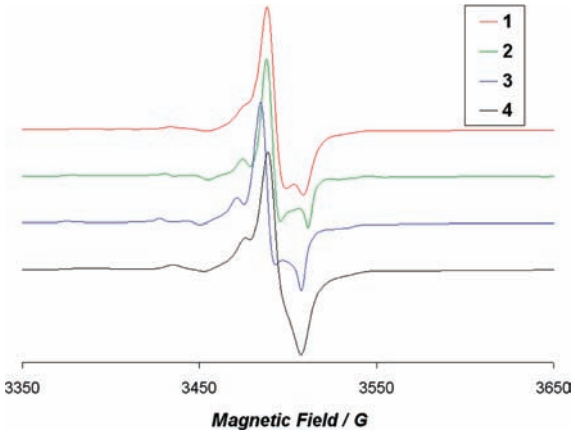

Figure 4. X-band EPR measurements registered at 77 K for **1**−**4**.

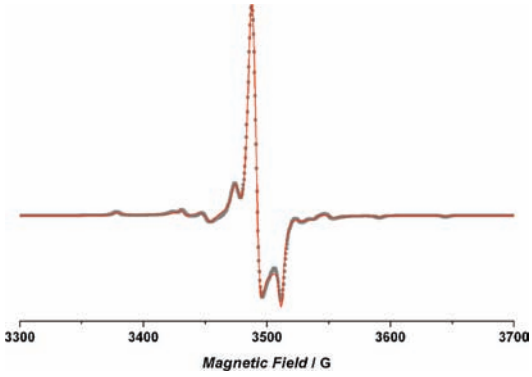

Figure 5. X-band EPR measurements at 77 K for **2**. Experimental data (gray dots) and best fit (red line) for Mo^{V} signal are presented (parameters in text).

neither observed at room temperature nor at 77 K. In the EPR measurements of **2a** at 4 K a very broad cobalt(II) signal without HFS (average effective g-factor about 3.6) is observed (Supporting Information, Figure S9). The presence of only one line in the EPR spectrum can be rationalized by the assumption of a very large zero field splitting. The spectrum is described by the effective spin $S = 1/2$, which is caused by the occupation of the ground Kramers doublet only.[59] The observed EPR parameters indicate that Co^{2+} is in high spin state in $[Co^{II}(bpy)_3]^{2+}$ complex. The EPR spectra recorded at 4 K confirm the presence of Mo^{V} for both, original (Supporting Information, Figure S10) and dehydrated samples (Supporting Information, Figure S9).

Magnetic Behavior. Below the temperature of 300 K, the compounds **1**−**4** are diamagnetic with very small paramagnetic contribution (at 250 K χT values are equal to 0.003 $cm^3\ mol^{-1}$ K for **2**, 0.016 $cm^3\ mol^{-1}$ K for **3**, and 0.023 $cm^3\ mol^{-1}$ K for **4**). While heating the samples up to 340−350 K during magnetic measurements (**2a**−**4a** compounds are formed), a significant increase of magnetization is observed, and the samples become paramagnetic. Continuous heating at 355 K for at least 4 h leads to the saturation of χT at the value of 1.45 $cm^3\ mol^{-1}$ K for **2a**, 1.41 $cm^3\ mol^{-1}$ K for **3a** and 1.29 $cm^3\ mol^{-1}$ K for **4a**

(59) Kusigerski, V. B.; Spasojević, V. V.; Lazarov, N. Dj.; Marković, D. S.; Matić, V. M.; Sovilj, S. P.; Guillot, M. *Solid State Commun.* **2003**, *126*, 319–322.

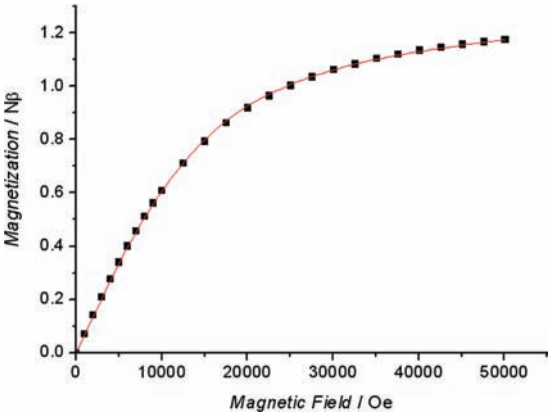

Figure 6. Magnetization vs magnetic field plot (squares) and best fit of Brillouin function (red line, parameters in text) for **2a**.

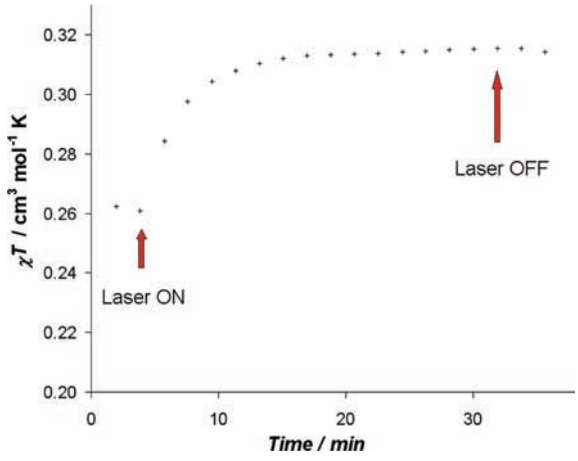

Figure 7. Time evolution of the magnetic signal in the form of χT product during irradiation of **2a′** with laser light λ = 647 nm at 10 K. The signal is corrected to reduce the temperature effect.

(Supporting Information, Figure S11). As an example, the dependence of χT versus T for **2a** is presented in the Supporting Information, Figure S12. The dramatic increase of paramagnetic signal is attributed to the thermal formation of Co^{II} and Mo^{V} centers. As the expected χT values at high temperature are equal to 3.54 $cm^3\ mol^{-1}$ K (assuming full conversion to Co^{II} − Mo^{V} system, $S_{Co} = 3/2$, $g_{Co} = 2.6$,[48] $S_{Mo} = 1/2$, $g_{Mo} = 1.99$), it is apparent that the conversion yield is of approximately 41%, 40%, and 36% for **2a**, **3a**, and **4a**, respectively. The numerical fitting with the Brillouin function of the field dependence of magnetization at 2 K, taking into account the partial conversion and assuming the effective spin of cobalt(II) in low temperature $S_{Co} = 1/2$, was performed to estimate the effective g-factor and the conversion yield. Such a fitting for compound **2a** (Figure 6) produces the following parameters: $g_{Co} = 4.1 \pm 0.4$ and conversion degree 43% ± 4% (constrained parameters $S_{Mo} = 1/2$, $g_{Mo} = 1.99$) which is in very good agreement with the value of magnetization observed at high temperature. The magnetic measurements on rehydrated compounds **1b**−**4b** showed that these materials are again diamagnetic. These magnetic results are in good agreement with the EPR data.

Photomagnetic Studies. Because the two valence forms Mo^{IV}−Co^{III} and Mo^{V}−Co^{II} of the compounds described

Table 5. Quantitative EPR Measurements Results for **1**−**4** and **1a**−**4a**

	1	**2**	**3**	**4**	**1a**	**2a**	**3a**	**4a**
total amount of molybdenum in the sample (mass percentage, calc.)	9.76	9.45	9.04	8.80	11.44	11.02	10.46	9.95
amount of molybdenum(V) in the sample (mass percentage, exp.)	0.27	0.05	0.11	0.22	4.34	2.56	1.91	2.10
amount of molybdenum(V) in the sample (% per all Mo centers, exp.)	**2.78**	**0.52**	**1.21**	**2.56**	**37.94**	**23.21**	**18.28**	**21.08**

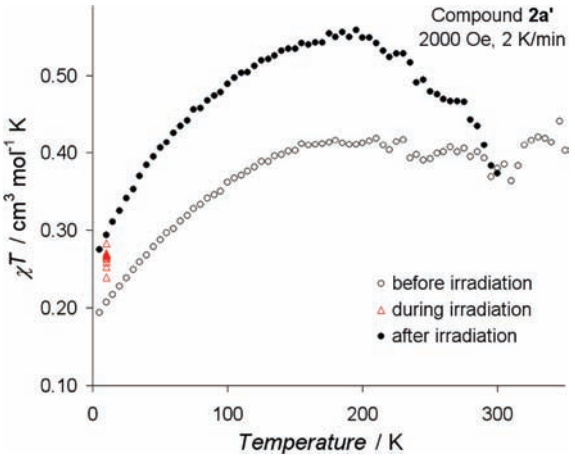

Figure 8. Photomagnetic properties of **2a**′ (compound **2** heated in SQUID cavity for 1 h at 355 K).

in this paper are close in energy, we tested the possibility to trap the metastable state $Mo^{V}-Co^{II}$ by irradiation in the MMCT band range. During irradiation at 10 K of **2** with light from the MMCT band (λ = 647 nm, ca. 30 mW/cm^2), no effect is observed. The situation is different for a partially anhydrous compound of **2**, noted hereafter **2a**′, obtained after 60 min in the SQUID cavity at 350 K. This compound shows a decrease of χT from 0.42 cm^3 mol^{-1}K at 350 K to 0.2 cm^3 mol^{-1}K at 5 K. This decrease may be attributed to the spin orbit coupling in the $[Co^{II}(bipy)_3]^{2+}$, as already reported for this complex.[60−64] The red light irradiation at 10 K causes an increase of the magnetization (ca. 20% of the signal value after 40 min of irradiation, Figure 7). This shows the existence of a photomagnetic effect for amorphous and dehydrated phase while no effect is observed for original sample. Then, after irradiation, we performed a magnetic characterization of the photoinduced state. Figure 8 shows that the photoinduced state is stable up to about 220 K, and in higher temperature it relaxes slowly reaching stability at 290 K at the level of the paramagnetic signal before irradiation.

Changes of the EPR signal during irradiation of the partially dehydrated sample **2a** (irradiation with red light 620 nm, ca. 20 mW/cm^2 at 4 K for 10 min.) were investigated. A small increase of the signal intensity was observed in both molybdenum and cobalt region (Figure 9). However, there is no visible change in the shape of the spectrum.

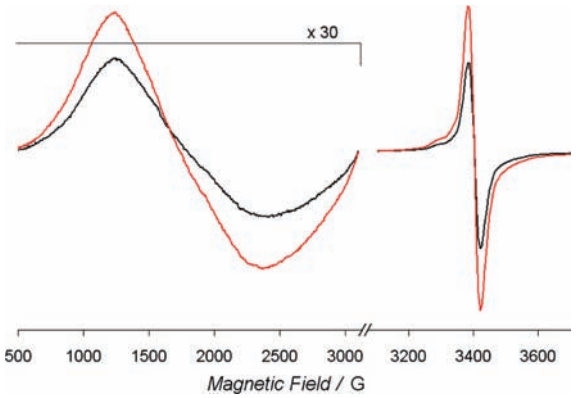

Figure 9. X-band EPR spectrum for **2a** registered at 4 K before (black) and after (red) irradiation with laser light λ = 647 nm for 10 min.

Scheme 1

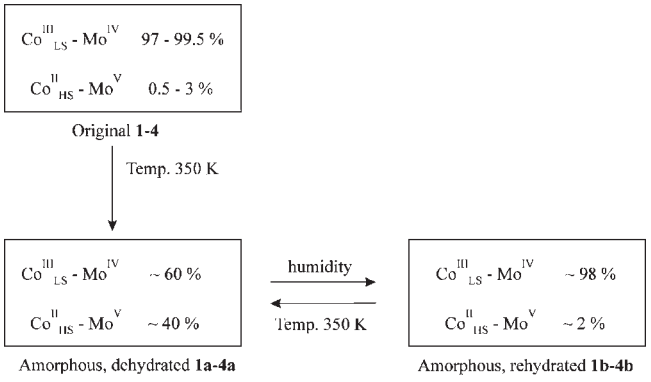

Discussion

In the solid state the equilibrium between the two electronic isomers $M[Co^{III}(bpy)_3][Mo^{IV}(CN)_8]\cdot nH_2O$ and $M[Co^{II}(bpy)_3][Mo^{V}(CN)_8]\cdot nH_2O$ has been observed, and it could be easily followed by the magnetic, XPS, and EPR measurements (Scheme 1). The original compounds **1**−**4** are practically diamagnetic because of the domination of the $Co^{III}Mo^{IV}$ isomer over the $Co^{II}Mo^{V}$ one (0.5−2.7%). During heating at 340−350 K the increase in the amount of paramagnetic phase up to 30−40% is observed. This phenomenon has been interpreted in terms of the loss of water molecules leading to the lowering of the charge transfer energy barrier and the shifting of the equilibrium toward the Co^{II} and Mo^{V} centers. This process is reversible, as upon the rehydration a return to diamagnetic form was observed. After cooling the dehydrated paramagnetic phase **2a**′ down to 10 K in the SQUID cavity, a photomagnetic effect (20%), *not seen* in the case of the original **2** phase, was observed. One of possible explanations is that a photoinduced charge transfer enhances the $Co^{III}{}_{LS}Mo^{IV} \rightarrow Co^{II}{}_{HS}Mo^{V}$ equilibrium shift. This photoreaction leads to exceeding equilibrium state forming "supersaturated" paramagnetic phase. A stable profile of the EPR signal confirms that there is apparently no other stable form in the system than the two already

(60) Lloret, F.; Julve, M.; Cano, J.; Ruiz-Garcia, R.; Pardo, E. *Inorg. Chim. Acta* **2008**, *361*, 3432–3445.
(61) Sieber, R.; Decurtins, S.; Stoeckli-Evans, H.; Wilson, C.; Yufit, D.; Howard, J. A. K.; Capelli, S. C.; Hauser, A. *Chem.—Eur. J.* **2000**, *6*, 361–368.
(62) Palmer, R. A.; Piper, T. S. *Inorg. Chem.* **1966**, *5*, 864–878.
(63) Figgis, B. N.; Lewis, J. The Magnetic Properties of Transition Metal Complexes. In *Progress in Inorganic Chemistry*; Cotton, E. A., Ed.; Interscience Publishers: New York, 1964; Vol. *6*, p 37.
(64) Kahn, O. *Molecular Magnetism*; VCH: New York, 1993

mentioned. Below 220 K the charge transfer between the two isomers seems to be quenched. Above this temperature slow relaxation to equilibrium state occurs.

The reasons why the photomagnetic effect is not observed in the case of the original crystalline compound **2** may have different origins: the rigidity of the crystalline network and also the presence of water molecules. Actually, the surroundings of the Co and Mo ions could not adjust to the new oxidation states of the cations and the anions in a rigid and compact structure. It is known that the coordination sphere of $Co^{III}N_6$ is smaller than the one of $Co^{II}N_6$.[47,48,65] Moreover, the presence or absence of water molecules may influence the redox potentials of each complex, and renders the $Co^{II}-Mo^{V}$ couple unstable. The loss of a periodical structure makes the system more flexible and favors the second electronic isomer which is formed in high temperature and may be formed in low temperature by photoexcitation.

Conclusions

The presented series of ionic compounds of general formula $M^{I}[Co(bpy)_3][Mo(CN)_8]\cdot nH_2O$ (M^{I} = Li, n = 8 (**1**), M^{I} = K, n = 8 (**2**), M^{I} = Rb, n = 8 (**3**), M^{I} = Cs, n = 7.5 (**4**)) shows the first example of a $Co^{III/II}$-$[Mo^{IV/V}(CN)_8]$ system with a tunable equilibrium between the $Co^{III}-Mo^{IV}$ and the $Co^{II}-Mo^{V}$ electronic isomers. The solvent removal not only decreases the energy barrier of this equilibrium allowing the change of the overall magnetic state but also enables the observation of photomagnetic effects. Furthermore, a metastable paramagnetic phase obtained in that manner is relatively stable in SQUID conditions up to T of 220 K (Figure 8). The samples exposed to ambient conditions or moisture return to diamagnetic states. These purely ionic systems might be relevant for the studies of functionality of cyano-bridged $Co^{III/II}$-$[Mo^{V/IV}(CN)_8]$ systems.

Acknowledgment. This work was partially supported by the EC within NoE project MAGMANet (Contract No. NMP3-CT-2005-515767) and by the Polish Ministry of Science and Higher Education within Research Project 1535/B/H03/2009/36. Thanks are due to G. Molnár, N. Ould Moussa, and L. Rechignat for the low-temperature EPR measurements.

Supporting Information Available: Crystallographic information files (CIF) for compounds **2** and **3**; experimental results: TGA and UV−vis for **2**, FT-IR for **1**−**4** and **1a**−**4a**, XPS for **1a**, **3a**, **4a**, magnetic experiment for **2**−**4** at 355 K, magnetic characterization of **2a** versus T (DOC). This material is available free of charge via the Internet at http://pubs.acs.org.

(65) Goodwin, H. A. Spin Crossover in Cobalt(II) Systems. In *Topics in Current Chemistry*; Gütlich, P., Goodwin, H. A., Eds.; Springer: Berlin, 2004; Vol. *234*, pp 23−47